Monitoring the Distribution of Mangrove Area using Synthetic Aperture Radar (SAR) and Optic Remote Sensing Data Fusion based on Deep Learning in Kotabaru Regency, Indonesia

Sudiana, Dodi
Department of Electrical Engineering, Faculty of Engineering, Universitas Indonesia

Nisa, Jamilatun
Department of Electrical Engineering, Faculty of Engineering, Universitas Indonesia

Rizkinia, Mia
Department of Electrical Engineering, Faculty of Engineering, Universitas Indonesia

Ratih Dewanti Dimyati
Research Center for Remote Sensing, National Research and Innovation Agency

他

https://doi.org/10.5109/7172320

出版情報：Evergreen. 11 (1), pp.536-546, 2024-03. 九州大学グリーンテクノロジー研究教育センター
バージョン：

Monitoring the Distribution of Mangrove Area using Synthetic Aperture Radar (SAR) and Optic Remote Sensing Data Fusion based on Deep Learning in Kotabaru Regency, Indonesia

Dodi Sudiana[1,2*], Jamilatun Nisa[1], Mia Rizkinia[1,2], Ratih Dewanti Dimyati[3], Nanin Anggraini[3], Indra Riyanto[4,2], Anton Satria Prabuwono[5,4], Josaphat Tetuko Sri Sumantyo[6]

[1] Department of Electrical Engineering, Faculty of Engineering, Universitas Indonesia, Indonesia
[2] Artificial Intelligence and Data Engineering Research Center (AIDE-RC), Faculty of Engineering, Universitas Indonesia, Indonesia
[3] Research Center for Remote Sensing, National Research and Innovation Agency, Indonesia
[4] Center for Environmental Studies, Universitas Budi Luhur, Indonesia
[5] Department of Information Technology, Faculty of Computing and Information Technology, Rabigh King Abdulaziz University, Saudi Arabia
[6] Center for Environmental Remote Sensing and Research Institute of Disaster Medicine, Chiba University, Japan

*Author to whom correspondence should be addressed:
E-mail: dodi.sudiana@ui.ac.id

(Received October 21, 2023; Revised January 31, 2024; Accepted March 05, 2024).

Abstract: Mangrove plants are crucial in providing ecosystem benefits that align with the Sustainable Development Goals (SDGs), particularly regarding climate regulation (SDG 13), due to their efficient carbon storage capabilities. Ensuring the preservation and effective management of this valuable natural resource requires precise mapping and monitoring systems. While mapping techniques using optical and radar remote sensing data have been utilized for monitoring mangrove areas, traditional methods for detecting mangrove damage face limitations concerning accuracy, efficiency, and automation. This research records a novel approach to mapping and monitoring mangrove ecosystems in Kotabaru Regency, South Kalimantan, from 2017 to 2021, using a fusion of Sentinel-1 and Sentinel-2 remote sensing satellite imagery data. The study demonstrates that the optimal combination of single-date Sentinel-1 and Sentinel-2 image inputs for mangrove identification in the deep learning model involves fusing Sentinel-2's original five-band data (Red, Green, Blue, NIR, and SWIR-1), four multispectral indices (FDI, MDI, MNDWI, and WFI), and Sentinel-1 SAR data (VV and VH). This fusion yields impressive performance metrics, including Overall Accuracy (OA) of 95.60%, Intersection over Union (IoU) of 93.09%, and F1-Score of 96.42%. Furthermore, the proposed optimal combination is utilized in this study to analyze the spatial-temporal dynamics of mangrove habitats in the study area every year from 2017 to 2021. The results reveal that the largest mangrove area in the study region was recorded as 8,240.06 hectares in 2019, while the smallest area was 7,069.68 hectares in 2020. This study demonstrates the potential of the proposed method as a valuable tool for accurate and efficient mangrove monitoring, providing critical information for effective conservation and management efforts.

Keywords: deep learning; image fusion; mangrove monitoring; Sentinel-1; Sentinel-2; Synthetic Aperture Radar (SAR)

1. Introduction

Deep learning has emerged as a pivotal and multifaceted tool across various domains of scientific inquiry. Its applications extend throughout diverse fields, demonstrating its utility. In pharmaceutical research, deep learning models have been harnessed to predict the intricate mechanical properties of substances like lactic acid[1], paving the way for enhanced material analysis. Developing deep learning algorithms for meteorology has revolutionized our ability to forecast wind patterns and weather conditions with remarkable precision[2], contributing to a deeper understanding of atmospheric dynamics. Economists have harnessed the power of deep learning to discern intricate patterns within the complex realm of metal prices, thus providing invaluable insights for market analysis and decision-making[3]. In safety and transportation, deep learning techniques have been instrumental in the development of systems capable of detecting driver fatigue and distraction, enhancing road safety and accident prevention[4]. In the realm of solar forecasting, the use of neural networks, which are a fundamental part of deep learning, has proven beneficial for assessing the Clearness Index, which provides crucial details about the atmospheric conditions for a particular location and is calculated as a ratio of the solar radiation from Space against the solar radiation from Earth[5,6]. The pervasive influence of deep learning underscores its profound impact on the advancement of knowledge and the optimization of various aspects of human life.

Indonesia has the largest mangrove ecosystem in the world[7]. Mangroves in Indonesia are a major focus of environmental development and contribute significantly to efforts to mitigate climate change[8]. Mangrove ecosystems in coastal areas are influenced by the tide and their ecosystems contribute directly or indirectly to achieving Sustainable Development Goals (SDGs). The mangrove ecosystems have a significant effect on climate and are acknowledged as major contributors to the "blue carbon sink" in coastal regions, which aids in diminishing atmospheric carbon dioxide emissions—a key indicator of climate change (SDG 13)[9]. These ecosystems also create a habitat for marine life and organisms (SDG 14) while benefiting society by providing fish and fishing grounds in coastal areas (SDG 2)[10] and shielding coastal areas from strong winds and waves[11].

Despite their vital role, in the 21st century, global mangrove habitats have continued to be damaged, mostly as a result of human activities[12]. Previous research has shown that global mangrove coverage decreased by 8,600 square kilometers between 1990 and 2020, with South and Southeast Asia experiencing the largest drop (3,870 square kilometers)[13]. Mangrove habitats are complex environments, and changes to tidal ebb and flow in the intertidal region adversely affect large-scale field surveys[14]. The complex nature of these ecosystems, with their intricate root systems and varied topography, poses challenges for accurate data collection during large-scale field studies. In order to protect and manage mangrove resources, monitoring needs to be carried out using methods that are effective and efficient in terms of time, cost, and manpower, by making use of remote sensing satellites[15]. Remote sensing analyses are less expensive in labor and time than field surveys and aerial photography, and they can be readily expanded to larger scales[16]. Remote Sensing techniques are widely used to monitor the environment and natural resources over extended periods[17,18], for purposes such as land cover classification[19,20], urban planning[21,22], traffic monitoring[23,24], and land cover change detection[25,26]. In many tropical regions, remote sensing is crucial to coastal monitoring because detailed estimates of changes in forest cover are necessary due to the effects these changes have on the environment and on sustainable development[27]. Over the last three decades, research on mangrove forests has been carried out using optical satellites and satellites equipped with Synthetic Aperture Radar (SAR), such as Landsat, IKONOS, QuickBird, ALOS PALSAR, Sentinel-1, and Sentinel-2.

Optical data, such as medium-resolution multispectral images from Landsat, are the most commonly used data for mangrove research. Jamaluddin et al.[28] used Landsat data and the Random Forest method to monitor mangrove forest degradation in East Luwu, Indonesia, over 20 years. Similarly, He et al.[29] used Landsat data to assess the extent of mangrove protection in the Guangdong—Hong Kong—Macao Greater Bay area.

However, the coastal areas of the tropics and parts of the subtropics are characterized by complex land cover types, while frequent cloudy or foggy days affect the availability of optical imagery. SAR satellite imagery offers high resolution and wide coverage and is not limited by climate and meteorological conditions except for extreme weather, which means that it can obtain periodic data on a regular basis. The study by Moreno et al.[30] found that Sentinel-1 (SAR) polarizations are effective for monitoring mangrove areas using deep learning techniques. Nevertheless, SAR images have problems with noise, shadows, overlapping pictures, and low signal-to-noise ratio. These limit the accuracy of identifying mangroves using SAR data only, but it is possible to use them as complementary image data in combination with optical images. Combining (fusing) SAR and optical data can improve the accuracy of mangrove area identification and classification[31].

Shallow machine learning classifiers such as Support Vector Machine (SVM), Random Forest (RF), etc., have become standard algorithms for mangrove mapping. Rijal et al.[32] mapped mangrove above-ground carbon using a machine-learning approach in Loh Buaya, Komodo National Park, Indonesia. Hu et al.[33] mapped China's mangrove forests using the Random Forest method, combining data from Sentinel-1 and Sentinel-2. However, deep learning (DL) remote sensing applications are rapidly gaining importance due to technological

advancements and the increasing accessibility of high-performance computing[34,35]. The existing literature shows that accurate maps of mangrove areas can be produced by applying DL or non-DL models to analyze information primarily derived from earth observation data (such as SAR and optical imagery). However, there is limited information that answers questions about mangrove mapping in DL modeling.

This study uses a deep-learning model to evaluate several single-sensor and multisensor approaches for mangrove mapping. Using Google Earth Engine (GEE) as the data processing platform and the Convolutional Neural Network (CNN) U-Net model, we propose a workflow that accurately identifies mangrove areas using single-date Sentinel-1 SAR and Sentinel-2 optical image fusion. This study addressed three research objectives:

1. Developing a mangrove-mapping method for the Kotabaru Regency using single-date Sentinel-1 and Sentinel-2 remote sensing image fusion data.
2. Evaluating the optimal combination of single-date image input data from Sentinel-1 and Sentinel-2 for identifying mangrove areas in a deep learning model to obtain accurate mangrove maps.
3. Analyzing changes in mangrove areas from 2017 to 2021 in Kotabaru Regency, Indonesia, as part of the national mangrove ecosystem monitoring system, for case study purposes.

2. Materials and Methods

2.1 Study Area and Data

The case study area is in Kotabaru Regency, South Kalimantan, Indonesia. This area has the largest mangrove ecosystem in South Kalimantan, covering 86,000 ha or around 73.62% of the total mangrove area. However, research results from the restoration and rehabilitation of mangrove forests in 2011 showed that they had lost around 76,092 ha or 65.13% of the total area[36,37].

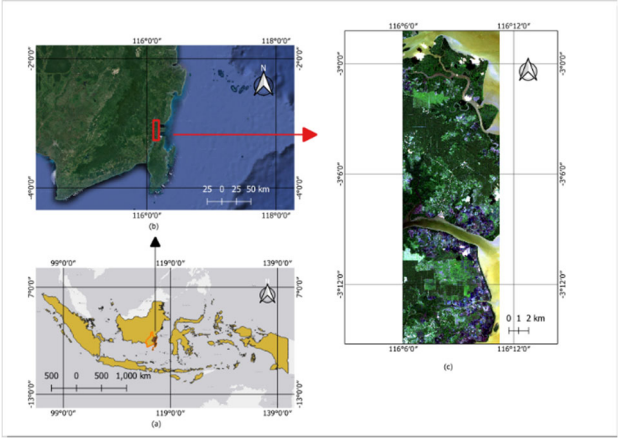

Fig. 1: Study Area in Kotabaru Regency. Sentinel-2 composite images (Red, Green, Blue).

Therefore, Kotabaru Regency was chosen as the study area based on its high rate of mangrove deforestation. It requires further analysis related to mangrove monitoring to determine the status and condition of the mangroves in this research area as part of the national mangrove ecosystem monitoring system. The area used in this study is shown in Fig. 1, which covers the Kelumpang Hilir, Kelumpang Hulu, and Pulau Laut Utara districts.

We used Sentinel-2 and Sentinel-1 single-date data in this study. The data was acquired through GEE. We selected Sentinel-2 Multispectral Instrument (MSI) data that has less than 5% of its pixels representing cloud. Table 1 shows the Sentinel-2 specifications in this study, including the acquisition dates.

Table 1. Sentinel-2 specifications.

Sensor	**Specifications**			
Sentinel-2 Multi-Spectral Instrument (MSI)	*Band*	**No.**	**Name**	**Resolution (m)**
		B3	Green (G)	10
		B4	Red (R)	10
		B8	Near Infrared (NIR)	10
		B11	Short Wave Infrared 1 (SWIR-1)	20
	Year	**Date**	**ID**	
	2017	15/06	COPERNICUS/S2/20170615T022551_20170615T024445_T50MMB	
	2018	22/02	COPERNICUS/S2/20180222T021709_20180222T023056_T50MMB	
	2019	03/05	COPERNICUS/S2/20190503T021611_20190503T023427_T50MLB	
	2020	21/01	COPERNICUS/S2/20200121T023011_20200121T024823_T50MLB	
	2021	21/06	COPERNICUS/S2/20210621T021601_20210621T023511_T50MLB	
	Product Level	L-2A		

Four multispectral indices, Modified Normalized Difference Water Index (MNDWI), Forest Discrimination Index (FDI), Wetland Forest Index (WFI), and Mangrove Discrimination Index (MDI), were obtained via band calculations for mangrove identification. The details of the calculation and formula are shown in Table 2.

MNDWI is an algorithm that clearly distinguishes between water and land, with an accuracy rate of 99.85% in extracting water information. The MNDWI calculates

the normalized difference between the green channel and the Short-wave Infrared 1 (SWIR-1) channel, emphasizing spectral variations that indicate the presence of liquid water[38]. FDI is the algorithm for extracting forest area information from remote sensing data. FDI uses Near-Infrared (NIR), red, and green channels to separate vegetation and non-vegetation features[39]. WFI is an algorithm used to identify vegetation in wetlands and muddy areas. The WFI calculates the normalized difference between Near-Infrared (NIR) and Red channels, divided by the Short-wave Infrared 2 (SWIR-2) channel[40]. Meanwhile, MDI is an algorithm used to estimate mangrove density. The MDI calculates the normalized difference between NIR and SWIR-2 channels, divided by the SWIR-2 channel. Through specific band formulation of remote sensing data, some of these indices can separate mangrove and non-mangrove vegetation[41].

Table 2. Multispectral indices.

Indices	Calculation	Formula in Sentinel-2
MNDWI[38]	$\frac{(\text{Green}-\text{SWIR1})}{(\text{Green}+\text{SWIR1})}$	$\frac{(\text{B3}-\text{B11})}{(\text{B3}+\text{B11})}$
FDI[39]	$\text{NIR}-(\text{Red}+\text{Green})$	$\text{B8}-(\text{B4}+\text{B3})$
WFI[40]	$\frac{(\text{NIR}-\text{Red})}{\text{SWIR2}}$	$\frac{(\text{B8}-\text{B4})}{\text{B12}}$
MDI[41]	$\frac{(\text{NIR}-\text{SWIR2})}{\text{SWIR2}}$	$\frac{(\text{B8}-\text{B12})}{(\text{B12})}$

In this study, we obtained the single-date image of SAR Sentinel-1 Ground Range Detected (GRD) via GEE with a capture time close to the Sentinel-2 image and subjected it to six stages of pre-processing: thermal noise removal, radiometric calibration, terrain correction, GRD border noise removal, and speckle filtering. Table 3 shows the Sentinel-1 specifications in this study, including the dates of acquisition.

Table 3. Sentinel-1 specifications.

Sensor	Year	Date	ID
Sentinel-1 (C-band SAR)	2017	10/06	COPERNICUS/S1_GRD/S1A_IW_GRDH_1SDV_20170610T215938_20170610T220003_016977_01C439_EFE9
	2018	17/02	COPERNICUS/S1_GRD/S1A_IW_GRDH_1SDV_20180217T215940_20180217T220005_020652_0235DF_44F7
	2019	02/05	COPERNICUS/S1_GRD/S1A_IW_GRDH_1SDV_20190502T215148_20190502T215213_027054_030C27_E39C
	2020	21/01	COPERNICUS/S1_GRD/S1A_IW_GRDH_1SDV_20200121T215153_20200121T215218_030904_038C12_F680
	2021	21/06	COPERNICUS/S1_GRD/S1A_IW_GRDH_1SDV_20210601T220002_20210601T220027_038152_0480C1_0BD2
	Specifications		
	Product Type		Ground Range Detected (GRD)
	Frequency		5.405 GHz
	Orbit		Descending
	Acquisition Method		Interferometric Wide (IW) swath
	Polarization Method		Vertical transmit-Vertical receive (VV), Vertical transmit-Horizontal receive (VH)

We used the 2021 map of Indonesia's mangrove areas provided by the Ministry of Environment and Forestry (MoEF) as ground truth data to label mangrove and non-mangrove samples in the dataset. Field sampling and visual interpretation of high-resolution satellite data are used to determine the ground truth. The ground truth is labeled manually under the supervision of several experts in mangrove mapping to ensure that the marked sample is correct. Figure 2 shows the reference (ground truth) data: white indicates a mangrove label, and black indicates a non-mangrove label.

Fig. 2: Ground truth map of mangrove area as reference data[42].

2.2 Methodology

Several data processing steps are required to map the mangrove areas. The workflow used by this study is depicted in Fig. 3. The first step involves the acquisition, pre-processing, and reprojection of Sentinel-1 and Sentinel-2 data using the GEE platform. Sentinel-1 data goes through a pre-processing stage that includes orbit file correction, GRD border noise removal, thermal noise removal, radiometric calibration, and terrain correction. Meanwhile, Sentinel-2 data is adjusted to standard size and normalized pixel values and divided into training, validation, and testing data. Next, optical data bands are

selected and SAR data polarization is carried out to form an input combination in the classification scheme. The CNN architecture is designed with a U-Net structure consisting of an encoder for extracting features from the input image and a decoder for reconstructing the output image from these features.

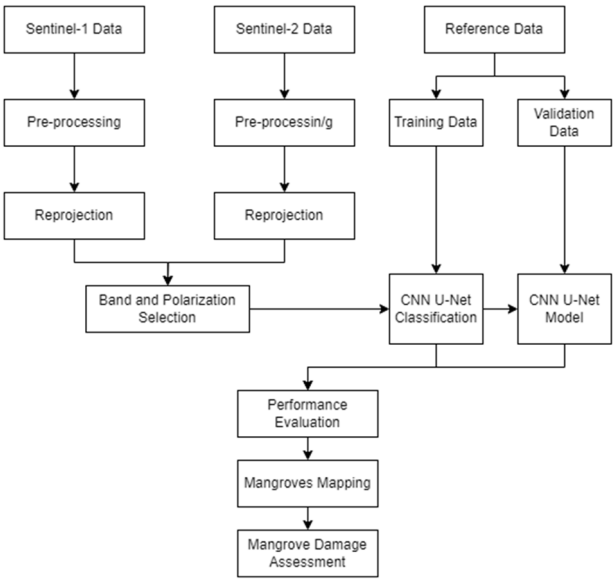

Fig. 3: Research workflow.

The next step includes a training and validation stage where the model is trained from reference data using the training and validation datasets. The output is in the form of mangrove/non-mangrove classification results. We used a test dataset for model evaluation to assess its generalization capabilities and determine its accuracy in classifying mangrove forests. Classification performance is evaluated using accuracy metrics such as intersection over union (IoU), overall accuracy (OA), and F1-Score. Finally, in the prediction and assessment stage, the trained model is used to classify mangrove/non-mangrove areas based on new satellite images, enabling prediction and assessment of mangrove damage.

2.3 U-Net

The CNN U-Net architecture[43] is known for its effectiveness in image segmentation tasks. U-Net is one of the most popular approaches in semantic segmentation, which divides images into "object" and "non-object." The original purpose of the U-net algorithm was biomedical image segmentation, targeting the segmentation of fine-grained class boundaries. However, it has also found application in conjunction with very high spatial-resolution imagery.

CNN U-net has encoder networks, bridges, and decoder networks. In the encoder, a series of 2D convolution operations is performed using a Conv2D layer with a continuously growing number of filters. After going through the Conv2D layer, Dropout is performed to prevent overfitting. Next, followed again by a Conv2D layer with the same number of filters, a max pooling operation using a MaxPooling2D layer is performed to reduce the spatial dimension.

The encoder network is then connected to the decoder network via a bridge that consists of two Conv2D layers and a Dropout between them. Furthermore, a reverse convolution operation is performed on the decoder network using Conv2DTranspose layers. Merging occurs using the concatenate layer between the Conv2DTranspose layer and the previous encoder layer with the same dimensions. Next, a series of 2D convolution operations are carried out using Conv2D with the same number of filters as in the encoder path, continued with the Dropout layer, and followed again by the Conv2D layer with the same number of filters. Each convolution layer on the U-Net layer uses ReLu and kernel activation size 3×3, and the Dropout layer uses a value of 0.5.

Finally, the 2D convolution operation is performed with a Conv2D layer with one filter and kernel size 1×1 to produce outputs with an activation function sigmoid to segment the image by generating the probability of each pixel.

2.4 Classification Schemes of Sentinel-1 and Sentinel-2 Image Band Combinations

Table 4 describes the segmentation scheme of the band combinations used as CNN U-Net inputs in this study. Bands and schemes are selected as inputs based on the ability of each band to identify mangrove and non-mangrove vegetation on the basis of their distinct characteristics. On Scheme #1, the input combination consists of the original five Sentinel-2 bands (Red, Green, Blue, NIR, SWIR-1). In Scheme #2, the input combination consists of four spectral indices for identifying mangroves, including MNDWI, FDI, WFI, and MDI. In Scheme #3, the input combination consists of Sentinel-1's two native bands: VV and VH. In Scheme #4, the input combination consists of the five original Sentinel-2 bands from Scheme #1 and the two original Sentinel-1 bands from Scheme #3. In Scheme #5, the input combination consists of the four spectral indices from Scheme #2 and Sentinel-1's two native bands from Scheme #3. Scheme #6 combines Schemes #1, #2, and #3, and consists of the five original Sentinel-2 bands, the four spectral indices, and the two original Sentinel-1 bands.

Table 4. Classification schemes.

Schemes	Bands	Descriptions	Total Inputs
#1	B2, B3, B4, B8 B11	Visible and Near Infrared (VNIR) Short Wave Infrared-1	5
#2	MNDWI FDI	Normalized Difference Water Index Forest Discrimination	4

	WFI MDI	Index Wetland Forest Index Mangrove Discrimination Index	
#3	VV VH	Vertical-Vertical polarization band Vertical-Horizontal polarization band	2
#4	Schemes (#1 + #3)	VNIR + SWIR-1 + SAR	7
#5	Schemes (#2 + #3)	Spectral Indices + SAR	6
#6	Schemes (#1 + #2 + #3)	VNIR + SWIR-1 + Spectral Indices + SAR	11

3. Results and Discussion

3.1 Data Preparation

We used the GEE to acquire and pre-process remote sensing data to produce multi-channel images for the research area, which we then downloaded locally. For the Sentinel-2 imagery, the image selected for training is a single image in 2021 with a cloud pixel percentage below 5%. We then took the band with a resolution of 20 meters per pixel and changed it to 10 meters per pixel. Meanwhile, for the Sentinel-1 image, we selected an image close in time to the Sentinel-2 image. Through GEE, Sentinel-1 imagery goes through several pre-processing stages, including thermal noise removal, radiometric calibration, field correction, orbit file correction, and GRD noise removal. The Sentinel-1 image also goes through a speckle filtering stage to reduce the speckle noise that generally occurs in radar images. Finally, we performed a reprojection on the Sentinel-1 image to cause it to have the same projection as the Sentinel-2 image.

We performed schematic input aggregation using the Sentinel Application Platform (SNAP) remote sensing software. Sentinel-1 and Sentinel-2 data underwent pre-processing, so they had the same 10-meter spatial resolution, range, and projection. At this stage, the collocation operator combines the input remote sensing data. This operator requires one reference product that defines the product's output range, pixel size, and pixel registration, and one or more secondary products to be cropped and resampled according to the reference product.

In Scheme #4, the input is a merging of input data of Scheme #1, which contains the five original Sentinel-2 bands (Red, Green, Blue, NIR, SWIR-1) as a reference product, and the input data of Schemes #2 and #3, which contain data from the four multispectral indices (MNDWI, FDI, WFI, MDI) and SAR data (VV and VH) as secondary products. The inputs in Scheme #4 are, therefore, Red, Green, Blue, NIR, SWIR-1, MNDWI, FDI, WFI, MDI VV, and VH. The reference data used is a map of Indonesia's mangrove areas for 2021. First, the reference data was converted from vector to raster and labeled mangrove and non-mangrove. After going through the pre-processing and merging stages, the size of the remote sensing data obtained was 975×3443 pixels for training and 559×803 pixels for testing. The remote sensing data was cropped into 128×128 pixels with a distance of 128 pixels to produce 113 training and 24 testing images. The training data is then augmented by flipping it horizontally and vertically and rotating it randomly by 90, 180, and 270 degrees so that the total training data is 452 images. Then, the training data is divided into training and validation data with a ratio of 70% (316 images) for training and 30% (126 images) for validation.

3.2 Hyperparameter Setting

The U-Net model is implemented using the Keras and TensorFlow frameworks provided by Google with Python through the Google Colaboratory. During the training of the U-Net model, the batch size used is 8, the number of training epochs is 100, and the number of iterations for each epoch is 40. The output layer uses the sigmoid function to meet the binary classification requirement. In addition, the Adam optimizer and loss function binary cross-entropy are used for learning.

3.3 Results and Analysis

The second research objective evaluates the optimal combination of optical and SAR remote sensing data by utilizing the U-Net model for mangrove mapping. We carried out the U-Net model experiments with the same hyperparameter settings. Table 5 and Figure 4 show the performance of the mangrove classification model using U-Net for schemes #1–#6, with the OA, IoU, and F1-Score as parameters.

Table 5. Test results.

Schemes	OA (%)	IoU (%)	F1-Score (%)
#1	95.13	92.67	96.19
#2	92.98	89.50	94.46
#3	79.49	68.79	81.51
#4	95.39	93.03	96.39
#5	95.10	92.49	96.10
#6	95.60	93.09	96.42

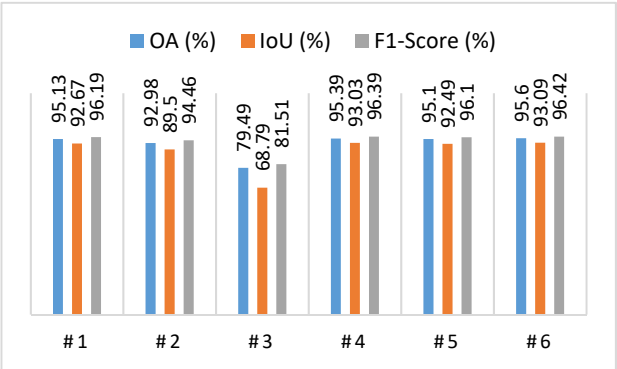

Fig. 4: Model performance graph for Schemes #1-#6.

In Scheme #1, the classification involves all spectral

bands (visible/RGB, NIR, and SWIR-1), resulting in OA, IoU, and F1-Score values of 95.13%, 92.67%, and 96.19%, respectively. The selection of these five bands is effective for mangrove identification because they have been adapted to the characteristics of mangrove vegetation. In Scheme #2, the classification involves four multispectral indices: MNDWI, FDI, WFI, and MDI, resulting in OA, IoU, and F1-Score values of 92.98%, 89.50%, and 94.46%, respectively. The selection of these four indices is also effective for mangrove identification because they have been adapted to the characteristics of mangrove vegetation. In scheme #3, the classification only involves SAR data (VV and VH) with OA, IoU, and F1-Score values of 79.49%, 68.79%, and 81.51%. Using SAR data alone results in the lowest evaluation metric values. This result shows that using SAR data alone is ineffective for identifying mangroves.

In Scheme #4, the classification involves a combination of the five original Sentinel-2 bands and SAR data (Schemes #1 + #3), resulting in OA, IoU, and F1-Score values of 95.39%, 93.03%, and 96.39%. The combination of Scheme #1 and Scheme #3 increases the OA, IoU, and F1-Score values by 0.26%, 0.36%, and 0.2%, respectively. In Scheme #5, the classification involves a combination of the four multispectral indices and SAR data (Schemes #2 + #3), resulting in OA, IoU, and F1-Score values of 95.10%, 92.49%, and 96.10%, respectively. This combination increases the OA, IoU, and F1-Score values by 2.12%, 2.99%, and 1.64%, respectively. In Scheme #6, the classification involves a combination of the five original Sentinel-2 bands, multispectral indices, and SAR data (Schemes #1 + #2 + #3), resulting in OA, IoU, and F1-Score values of 95.60%, 93.09%, and 96.42%, respectively. These results show that Scheme #6 produces the best model performance based on OA, IoU, and F1-Score parameters.

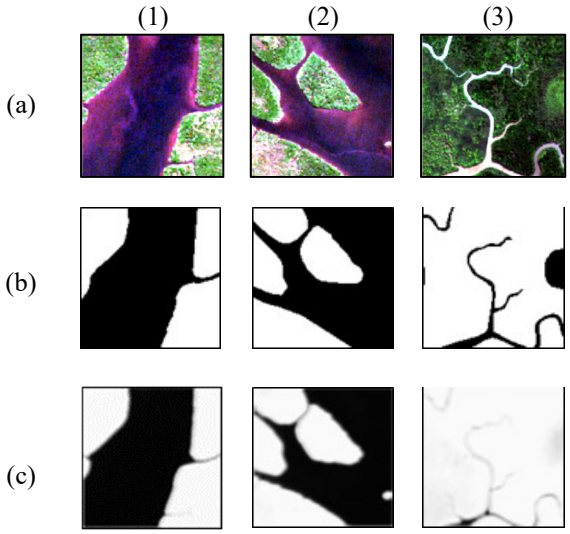

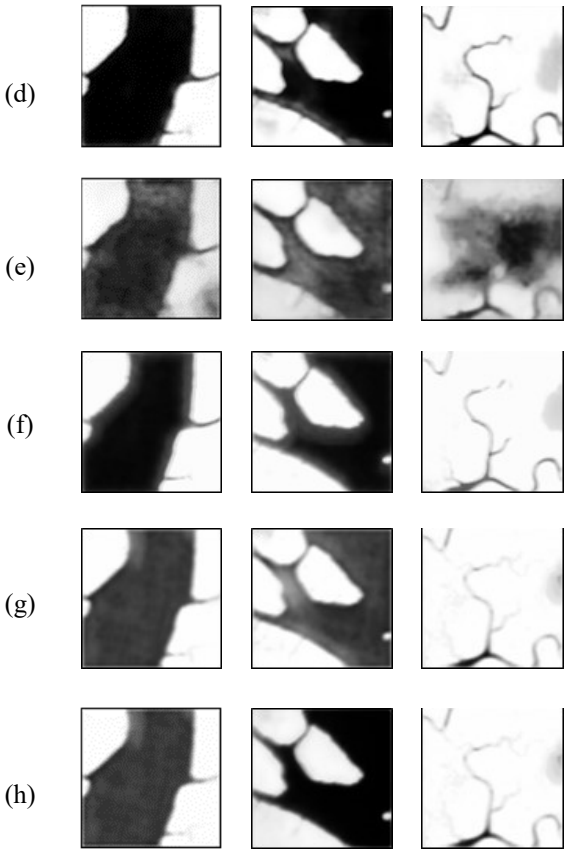

Fig. 5: Detailed information on mangrove identification results from Schemes #1–#6. Row (a) remote sensing imagery; Row (b) ground truth data; Rows (c–h) Schemes #1–#6. Columns (1)–(3) represent the classification subsets taken from the study area.

We selected three mangrove distribution areas as subsets of the area of interest for comparative analysis. Figure 5 shows the remote sensing images and the four schemes' identification results for the subset study areas. Scheme #3, as shown in Fig. 5(e), cannot accurately identify mangrove and non-mangrove areas. We can, therefore, conclude that using SAR data alone without adding other features and only conducting pixel-based pre-processing is ineffective using the U-Net method.

Figure 6(a)–(f) depicts the confusion matrix for schemes #1 to #6 using the U-Net model, showing how 393,216 pixels of test data were classified. The lowest performance classification in Scheme #3 includes only SAR data. In this scheme, there were 65,899 misclassifications of pixels as mangroves and 14,717 pixels as non-mangroves. However, 79.49% of the pixels in Scheme #3 are correctly classified. In scheme #6, visual classification with a combination of the five original Sentinel-2 bands, the multispectral indices, and the SAR data (VV and VH) produces the smallest FP (false positive) value compared to the other schemes, recorded at 6,352 pixels.

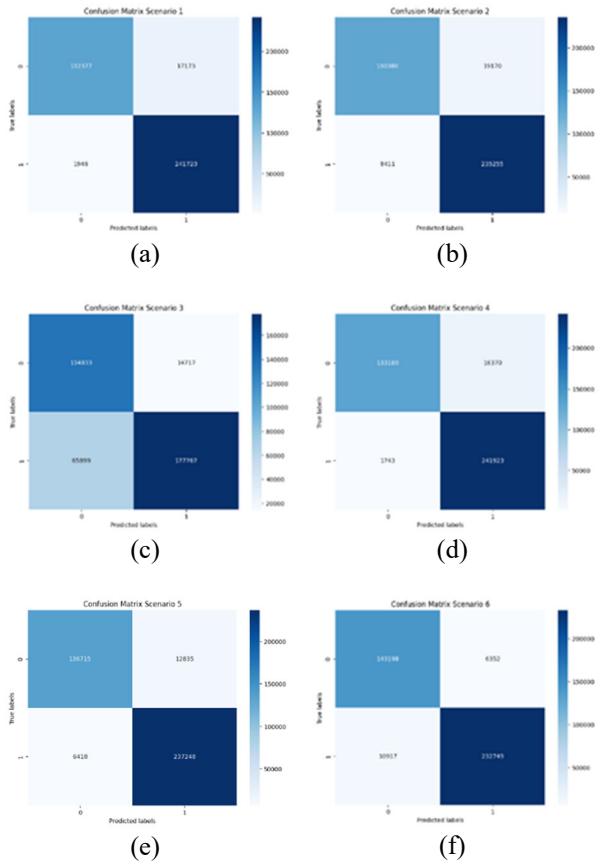

Fig. 6: Mangrove classification confusion matrix for: (a) Scheme #1; (b) Scheme #2; (c) Scheme #3; (d) Scheme #4; (e) Scheme #5; and (f) Scheme #6.

3.4 Analysis of Spatiotemporal Change in Mangroves-in the Study Area

Based on the results of the first and second research objectives, the optimal combination of data from optical and SAR remote sensing data for identifying mangroves is Scheme #6 with OA, IoU, and F1-Score values of 95.60%, 93.09%, and 96.42%. This result constitutes the primary model for mapping mangrove areas and analyzes changes in mangrove coverage annually in the study area from 2017 to 2021, as shown in Table 6.

Table 6. Mangrove area changes in the study area.

Date of observation	Mangrove area (Ha)
06/15/2017	8117.10
02/22/2018	7371.81
05/03/2019	8240.06
02/22/2020	7069.68
06/21/2021	8198.71

Figure 7 illustrates graphically the mangrove extent in Kotabaru Regency, Indonesia, from 2017 to 2021. The largest mangrove area in the regency occurred in 2019, with a total area of 8240.06 hectares. Conversely, the smallest mangrove area in the study area was in 2020, with a total area of 7069.68 hectares. This study's utilization of single-date data from each year enables us to calculate mangrove ecosystem extents at a specific time rather than representing periodic conditions. The significant variations in the mangrove ecosystem's extent, as depicted in the data, are influenced by factors such as climate change, human activities, and other environmental variables, providing profound insights into the dynamics of the mangrove ecosystem over the specified time. Nevertheless, the proposed method demonstrates its efficacy by delivering crucial information for stakeholders' effective conservation and management efforts.

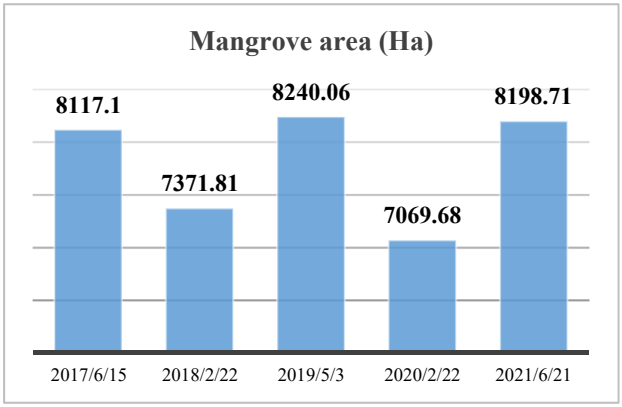

Fig. 7: Graph of mangrove extent in 2017-2021.

Compared with several studies that have utilized other methods[33, 44], this approach offers great potential in terms of accuracy. Hu et al.[33] used the Random Forest technique to map China's mangrove forests by fusing information from Sentinel-1 and Sentinel-2. The F1-Score for their study was 94%, compared to the 96.42% we obtained. Similarly, Ghorbanian et al.[44] mapped the mangrove ecosystem of the Hara protected area in Qeshm, Iran, by utilizing Sentinel-1 and Sentinel-2 data as inputs to their model and obtained an overall accuracy of 93.23%.

4. Conclusions

This study shows that the optimal combination of input data for identifying mangroves in the deep learning recognition model is a combination of the five original Sentinel-2 bands (Red, Green, Blue, NIR, and SWIR-1), four multispectral indices (FDI, MNDWI, MDI, and WFI), and SAR data (VV and VH) with OA, IoU, and F1-Score values of 95.60%, 93.09%, and 96.42%, respectively. Using this tool, we were able to determine that the largest mangrove area in the study area occurred in 2019, with a total area of 8240.06 hectares, while the smallest mangrove area in the study area occurred in 2020, with a total area of 7069.68 hectares.

Acknowledgments

This research is funded by the Directorate of Research Development, Universitas Indonesia, under Hibah PUTI Q2 2023 No. NKB-806/UN2.RST/HKP.05.00/2023.

References

1) J.F. Fatriansyah, S.N. Surip, and F. Hartoyo, "Mechanical property prediction of poly(lactic acid) blends using deep neural network," *Evergreen*, 9 (*1*) 141–144 (2022). doi:10.5109/4774229.
2) H. Halidah, N. Hesty, P. Aji, Ifanda, D. Amelia, and K. Akhmad, "Short-term wind forecasting with weather data using deep learning - case study in baron techno park," *Evergreen*, 10 (*3*) 1753–1761 (2023). doi:10.5109/7151724.
3) V. Aggarwal, A. Ranjan, S. Shaurya, and S.K. Garg, "To determine the futures pricing of metal commodities using deep learning," *Evergreen*, 10 (*2*) 1027–1033 (2023). doi:10.5109/6793658.
4) P. Panwar, P. Roshan, R. Singh, M. Rai, A.R. Mishra, and S.S. Chauhan, "DDNet- a deep learning approach to detect driver distraction and drowsiness," *Evergreen*, 9 (*3*) 881–892 (2022). doi:10.5109/4843120.
5) A. Al Karim Haj Ismail, "Prediction of global solar radiation from sunrise duration using regression functions," n.d.*Kuwait J of Sci*, 49 *(3)* 1-8 (2022). doi: 10.48129/kjs.15051
6) A.H. Ismail, E.A. Dawi, N. Almokdad, A. Abdelkader, and O. Salem, "Estimation and comparison of the clearness index using mathematical models - case study in the united arab emirates," *Evergreen*, 10 (*2*) 863–869 (2023). doi:10.5109/6792841.
7) M. Jia, Z. Wang, D. Mao, C. Ren, K. Song, C. Zhao, C. Wang, X. Xiao, and Y. Wang, "Mapping global distribution of mangrove forests at 10-m resolution," *Sci Bull (Beijing)*, 68 (*12*) 1306–1316 (2023). doi:10.1016/j.scib.2023.05.004.
8) A.D. Purwanto, K. Wikantika, A. Deliar, and S. Darmawan, "Decision tree and random forest classification algorithms for mangrove forest mapping in sembilang national park, indonesia," *Remote Sens (Basel)*, 15 (*1*) (2023). doi:10.3390/rs15010016.
9) Bory B. Alikhanov, Sergei V. Samoilov, Vadim I. Sokolov, and Leyli P. Seitova, "Theory of climate change intensity determination," *Evergreen*, 10 (*3*) 1253–1260 (2023). doi:10.5109/7148446.
10) S.D. Sasmito, M. Basyuni, A. Kridalaksana, M.F. Saragi-Sasmito, C.E. Lovelock, and D. Murdiyarso, "Challenges and opportunities for achieving sustainable development goals through restoration of indonesia's mangroves," *Nat Ecol Evol*, 7 (*1*) 62–70 (2023). doi:10.1038/s41559-022-01926-5.
11) C. Xu, J. Wang, Y. Sang, K. Li, J. Liu, and G. Yang, "An effective deep learning model for monitoring mangroves: a case study of the indus delta," *Remote Sens (Basel)*, 15 (*9*) (2023). doi:10.3390/rs15092220.
12) L. Goldberg, D. Lagomasino, N. Thomas, and T. Fatoyinbo, "Global declines in human-driven mangrove loss," *Glob Chang Biol*, 26 (*10*) 5844–5855 (2020). doi:10.1111/gcb.15275.
13) A.K. Bhowmik, R. Padmanaban, P. Cabral, and M.M. Romeiras, "Global mangrove deforestation and its interacting social-ecological drivers: a systematic review and synthesis," *Sustainability (Switzerland)*, 14 (*8*) (2022). doi:10.3390/su14084433.
14) X. Wang, L. Tan, and J. Fan, "Performance evaluation of mangrove species classification based on multi-source remote sensing data using extremely randomized trees in fucheng town, leizhou city, guangdong province," *Remote Sens (Basel)*, 15 (*5*) (2023). doi:10.3390/rs15051386.
15) K. Maurya, S. Mahajan, and N. Chaube, "Remote sensing techniques: mapping and monitoring of mangrove ecosystem—a review," *Complex and Intelligent Systems*, 7 (*6*) 2797–2818 (2021). doi:10.1007/s40747-021-00457-z.
16) P. Zheng, P. Fang, L. Wang, G. Ou, W. Xu, F. Dai, and Q. Dai, "Synergism of multi-modal data for mapping tree species distribution—a case study from a mountainous forest in southwest china," *Remote Sens (Basel)*, 15 (*4*) (2023). doi:10.3390/rs15040979.
17) A. Yussupov, and R.Z. Suleimenova, "Use of Remote Sensing Data for Environmental Monitoring of Desertification," *Evergreen*, 10 (*1*) 300–307 (2023). doi: doi.org/10.5109/6781080.
18) X. Liu, X. Yang, T. Zhang, Z. Wang, J. Zhang, Y. Liu, and B. Liu, "Remote sensing based conservation effectiveness evaluation of mangrove reserves in china," *Remote Sens (Basel)*, 14 (*6*) (2022). doi:10.3390/rs14061386.
19) R. Li, X. Gao, F. Shi, and H. Zhang, "Scale effect of land cover classification from multi-resolution satellite remote sensing data," *Sensors*, 23 (*13*) (2023). doi:10.3390/s23136136.
20) F. Hanif, S. Kanae, R. Farooq, M.R. Iqbal, and A. Petroselli, "Impact of satellite-derived land cover resolution using machine learning and hydrological simulations," *Remote Sens (Basel)*, 15 (*22*) 5338 (2023). doi:10.3390/rs15225338.
21) D. Gong, X. Dai, and L. Zhou, "Satellite-based optimization and planning of urban ventilation corridors for a healthy microclimate environment," *Sustainability*, 15 (*21*) 15653 (2023). doi:10.3390/su152115653.
22) X. Zhang, R. Ye, and X. Fu, "Assessment of urban local high-temperature disaster risk and the spatially heterogeneous impacts of blue-green space," *Atmosphere (Basel)*, 14 (*11*) 1652 (2023). doi:10.3390/atmos14111652.
23) M. Ragab, H.A. Abdushkour, A.O. Khadidos, A.M. Alshareef, K.H. Alyoubi, and A.O. Khadidos, "Improved deep learning-based vehicle detection for urban applications using remote sensing imagery," *Remote Sens (Basel)*, 15 (*19*) (2023). doi:10.3390/rs15194747.
24) T. Chen, J. Qi, M. Xu, L. Zhang, Y. Guo, and S. Wang,

"Deployment of remote sensing technologies for effective traffic monitoring," *Remote Sens (Basel)*, 15 (*19*) (2023). doi:10.3390/rs15194674.

25) Z. Wu, X. Zhang, P. Ma, M.-P. Kwan, and Y. Liu, "How did urban environmental characteristics influence land surface temperature in hong kong from 2017 to 2022? evidence from remote sensing and land use data," *Sustainability*, 15 (*21*) 15511 (2023). doi:10.3390/su152115511.
26) Y. Wu, and J. Pan, "Detecting changes in impervious surfaces using multisensor satellite imagery and machine learning methodology in a metropolitan area," *Remote Sens (Basel)*, 15 (*22*) 5387 (2023). doi:10.3390/rs15225387.
27) R. Morocho, I. González, T.O. Ferreira, and X.L. Otero, "Mangrove forests in ecuador: a two-decade analysis," *Forests*, 13 (*5*) (2022). doi:10.3390/f13050656.
28) I. Jamaluddin, Y.-N. Chen, S.M. Ridha, P. Mahyatar, and A.G. Ayudyanti, "Two decades mangroves loss monitoring using random forest and landsat data in east luwu, indonesia (2000–2020)," *Geomatics*, 2 (*3*) 282–296 (2022). doi:10.3390/geomatics2030016.
29) T. He, Y. Fu, H. Ding, W. Zheng, X. Huang, R. Li, and S. Wu, "Evaluation of mangrove wetlands protection patterns in the guangdong–hong kong–macao greater bay area using time-series landsat imageries," *Remote Sens (Basel)*, 14 (*23*) (2022). doi:10.3390/rs14236026.
30) G.M. de S. Moreno, O.A. de Carvalho Júnior, O.L.F. de Carvalho, and T.C. Andrade, "Deep semantic segmentation of mangroves in brazil combining spatial, temporal, and polarization data from sentinel-1 time series," *Ocean Coast Manag*, 231 (2023). doi:10.1016/j.ocecoaman.2022.106381.
31) K. Huang, G. Yang, Y. Yuan, W. Sun, X. Meng, and Y. Ge, "Optical and sar images combined mangrove index based on multi-feature fusion," *Science of Remote Sensing*, 5 100040 (2022). doi:10.1016/j.srs.2022.100040.
32) S.S. Rijal, T.D. Pham, S. Noer'Aulia, M.I. Putera, and N. Saintilan, "Mapping mangrove above-ground carbon using multi-source remote sensing data and machine learning approach in loh buaya, komodo national park, indonesia," *Forests*, 14 (*1*) (2023). doi:10.3390/f14010094.
33) L. Hu, N. Xu, J. Liang, Z. Li, L. Chen, and F. Zhao, "Advancing the mapping of mangrove forests at national-scale using sentinel-1 and sentinel-2 time-series data with google earth engine: a case study in china," *Remote Sens (Basel)*, 12 (*19*) (2020). doi:10.3390/RS12193120.
34) C. Fu, X. Song, Y. Xie, C. Wang, J. Luo, Y. Fang, B. Cao, and Z. Qiu, "Research on the spatiotemporal evolution of mangrove forests in the hainan island from 1991 to 2021 based on svm and res-unet algorithms," *Remote Sens (Basel)*, 14 (*21*) (2022). doi:10.3390/rs14215554.
35) D. Lomeo, and M. Singh, "Cloud-based monitoring and evaluation of the spatial-temporal distribution of southeast asia's mangroves using deep learning," *Remote Sens (Basel)*, 14 (*10*) (2022). doi:10.3390/rs14102291.
36) Baharuddin. "Analisis kekritisian lahan mangrove Kalimantan Selatan dengan menggunakan sistem informasi geografis dalam rangka pengelolaan konservasi lahan basah pesisir [Analysis of the criticality of South Kalimantan's mangrove land using a geographic information system in the context of coastal wetland conservation management]," Jurnal Enggano, 5(3) 495-509, (2021). doi:10.31186/jenggano.5.3.495-509.19.
37) Republik Indonesia, UU 5/1990 Tentang Konservasi Sumber Daya Alam Hayati dan Ekosistem; UU 27/2007 Pengelolaan Wilayah Pesisir dan Pulau-Pulau Kecil; Pasal 98 ayat (1) UU 32/2009 Tentang Perlindungan serta Pengelolaan Lingkungan Hidup; and Pasal 82 ayat (1) UU 1/2013. https://www.kompas.com/skola/read/2021/03/17/142637069/isi-aturan-tentang-lingkungan-hidup-uu-no-32-tahun-2009.
38) H. Xu, "Modification of normalised difference water index (ndwi) to enhance open water features in remotely sensed imagery," *Int J Remote Sens*, 27 (*14*) 3025–3033 (2006). doi:10.1080/01431160600589179.
39) M. Kamal, S. Phinn, and K. Johansen, "Object-based approach for multi-scale mangrove composition mapping using multi-resolution image datasets," *Remote Sens (Basel)*, 7 (*4*) 4753–4783 (2015). doi:10.3390/rs70404753.
40) D. Wang, B. Wan, P. Qiu, Y. Su, Q. Guo, R. Wang, F. Sun, and X. Wu, "Evaluating the performance of sentinel-2, landsat 8 and pléiades-1 in mapping mangrove extent and species," *Remote Sens (Basel)*, 10 (*9*) (2018). doi:10.3390/rs10091468.
41) M. Wang, W. Cao, Q. Guan, G. Wu, and F. Wang, "Assessing changes of mangrove forest in a coastal region of southeast china using multi-temporal satellite images," *Estuar Coast Shelf Sci*, 207 283–292 (2018). doi:10.1016/j.ecss.2018.04.021.
42) Menlhk.go.id, "Peta Mangrove Nasional Tahun 2021: Baseline Pengelolaan Rehabilitasi Mangrove Nasional [National Mangrove Map 2021: National Mangrove Rehabilitation Management Baseline]," Ministry of Environment and Forestry, https://www.menlhk.go.id/site/single_post/4476/peta-mangrove-nasional-tahun-2021-baseline-pengelolaan-rehabilitasi-mangrove-nasional
43) O. Ronneberger, P. Fischer, and T. Brox, "U-net: convolutional networks for biomedical image segmentation," *Lecture Notes in Computer Science (Including Subseries Lecture Notes in Artificial Intelligence and Lecture Notes in Bioinformatics)*,

9351 234–241 (2015). doi:10.1007/978-3-319-24574-4_28/COVER.

44) A. Ghorbanian, S. Zaghian, R.M. Asiyabi, M. Amani, A. Mohammadzadeh, and S. Jamali, "Mangrove ecosystem mapping using sentinel-1 and sentinel-2 satellite images and random forest algorithm in google earth engine," *Remote Sens (Basel)*, 13 (*13*) (2021). doi:10.3390/rs13132565.